JOURNAL OF THERMOPHYSICS AND HEAT TRANSFER
Vol. 16, No. 3, July–September 2002

# Analysis of Wire-Bonded Micro Heat Pipe Arrays

Y. X. Wang* and G. P. Peterson†
*Rensselaer Polytechnic Institute, Troy, New York 12180*

**Flat micro heat pipes utilizing arrays of parallel metal wires sandwiched between two thin metal sheets were conceptualized, modeled, and analyzed. An experimental facility was fabricated and experimental tests were conducted to verify the concept, as well as to validate the proposed model. The modeling results were then compared with the results of the experimental investigation. In the analytical portion of the investigation, a one-dimensional steady-state analytical model, which incorporated the effects of the liquid–vapor phase interaction and the variation in the cross-sectional area, was developed to predict the heat transfer performance and optimum design parameters. The mass distribution, optimum charge, and maximum heat transport capacity were all obtained by solving the one-dimensional governing equations numerically. The results indicated that the maximum heat transport capacity increased with increases in wire diameter and that the overall value was proportional to the square of the wire diameter. The wire diameter was also found to affect the optimum operating temperature within the overall operating temperature range of the working fluid. In addition to determining the effect of the wire diameter, the numerical model provided a mechanism by which the effects of the wire spacing and evaporator heat flux could be determined. The results indicated that the maximum heat transport capacity increased with increases in the wire spacing and that there exists an optimal configuration that yields the maximum heat transport capacity. The optimum charge volume was shown to decrease rapidly with increases in the evaporator heat flux. The results of the analytical model were compared with experimental results available in the literature and indicated good agreement between the predicted and measured maximum heat transport capacity for these types of wire-bonded flat heat pipes.**

## Nomenclature

| | | |
|---|---|---|
| $A_{c,l}$ | = | liquid-phase cross-sectional area, m$^2$ |
| $A_{c,v}$ | = | vapor-phase cross-sectional area, m$^2$ |
| $A_i$ | = | liquid–vapor interface cross-sectional area, m$^2$ |
| $A_{l,w}$ | = | liquid–wall contact area, m$^2$ |
| $A_{v,w}$ | = | vapor–wall contact area, m$^2$ |
| $C_p$ | = | specific heat capacity, J/kg K |
| $D_{h,l}$ | = | hydraulic diameter of liquid, m |
| $D_{h,v}$ | = | hydraulic diameter of vapor, m |
| $d_w$ | = | wire diameter, m |
| $f_l$ | = | liquid friction factor |
| $f_v$ | = | vapor friction factor |
| $g$ | = | gravity acceleration, m/s$^2$ |
| $H$ | = | height of the triangle, m |
| $h_{fg}$ | = | latent heat of vaporization, J/kg |
| $k_l$ | = | thermal conductivity of liquid, W/K · m |
| $k_v$ | = | thermal conductivity of vapor, W/K · m |
| $L_c$ | = | length of condenser section, m |
| $L_e$ | = | length of evaporator section, m |
| $L_t$ | = | total length of the micro heat pipe, m |
| $M$ | = | mass, kg |
| $m_l$ | = | liquid mass flow rate, kg/s |
| $m_v$ | = | vapor mass flow rate, kg/s |
| $P$ | = | pressure, Pa |
| $P_c$ | = | capillary pressure, Pa |
| $P_l$ | = | liquid pressure, Pa |
| $P_v$ | = | vapor pressure, Pa |
| $P_{v,0}$ | = | reference pressure, Pa |
| $p_{i,l}$ | = | liquid–vapor interfacial perimeter, m |
| $p_{i,v}$ | = | vapor–liquid interfacial perimeter, m |
| $p_l$ | = | liquid wetted perimeter, m |
| $p_v$ | = | vapor wetted perimeter, m |
| $Q$ | = | heat transport, W |
| $Q_{\max}$ | = | maximum heat transport capacity, W |
| $q_a$ | = | heat flux in adiabatic section, W/m$^2$ |
| $q_c$ | = | maximum heat transport capacity, W/m$^2$ |
| $q_e$ | = | maximum heat transport capacity, W/m$^2$ |
| $q''$ | = | heat flux per unit area, W/m$^2$ |
| $Re$ | = | Reynolds number |
| $R_w$ | = | radius of wire, m |
| $r_m$ | = | radius of liquid meniscus, m |
| $T$ | = | temperature, °C |
| $T_l$ | = | liquid temperature, °C |
| $T_{\text{ope}}$ | = | operation temperature, °C |
| $T_v$ | = | vapor temperature, °C |
| $T_{v,0}$ | = | reference temperature, °C |
| $u_l$ | = | liquid velocity in $x$ direction, m/s |
| $u_v$ | = | vapor velocity in $x$ direction, m/s |
| $V$ | = | volume, m$^3$ |
| $V_c$ | = | control volume, m$^3$ |
| $v_{i,l}$ | = | liquid velocity at interface, m/s |
| $v_{i,v}$ | = | vapor velocity at interface, m/s |
| $w$ | = | width of the single heat pipe, m |
| $\alpha$ | = | contact angle, grade |
| $\beta_1$ | = | half-angle of contact arc of liquid with wire, grade |
| $\beta_2$ | = | half-angle of liquid curvature, grade |
| $\theta$ | = | inclination angle, deg |
| $\mu_l$ | = | liquid viscosity, N · s/m$^2$ |
| $\mu_v$ | = | vapor viscosity, N · s/m$^2$ |
| $\nu_l$ | = | liquid dynamic viscosity, m$^2$/s |
| $\nu_v$ | = | vapor dynamic viscosity, m$^2$/s |
| $\xi$ | = | dimensionless geometry parameter |
| $\rho_l$ | = | liquid density, kg/m$^3$ |
| $\rho_v$ | = | vapor density, kg/m$^3$ |
| $\sigma$ | = | surface tension, N/m |
| $\tau$ | = | shear stress, N/m$^2$ |
| $\Psi$ | = | dimensionless shape factor |

Received 28 September 2001; revision received 2 February 2002; accepted for publication 12 February 2002. 

*Postdoctoral Research Associate, Department of Mechanical Aerospace and Nuclear Engineering. Member AIAA.

†Provost and Professor of Mechanical Engineering, Department of Mechanical Aerospace and Nuclear Engineering, Office of the Provost, Room 3018, Troy Building. Fellow AIAA.

*Subscripts*

| | | |
|---|---|---|
| $a$ | = | adiabatic |
| $c$ | = | condenser |
| cap | = | capillary |
| $e$ | = | evaporator |
| $l$ | = | liquid phase |
| $m$ | = | meniscus |
| max | = | maximum |
| min | = | minimum |
| $v$ | = | vapor phase |

## Introduction

FLAT plate heat pipes have been of interest for some time, but the recent advances in microscale flat plate heat pipes have resulted in a series of devices that could have wide-ranging applications in the areas of spacecraft thermal control and the thermal control of electronic equipment. The sheer size and weight, when combined with the ability to fabricate these devices in basically any shape and with limited flexibility, have made micro heat pipes a viable candidate for use in flexible and lightweight radiators or as heat spreaders in laptop computers. In the present investigation, a flexible, lightweight, wire-bonded micro heat pipe has been proposed, fabricated, and investigated experimentally. To better understand the operating characteristics and the heat transport limitations, and to optimize the physical characteristics, a theoretical analysis of these micro heat pipes was conducted.

A micro heat pipe is typically a wickless, noncircular channel with a channel radius approximately the same as the characteristic radius of the liquid meniscus.[1] Since 1984, several studies have been undertaken to better understand the effect of continued size reductions of micro heat pipes, determine the effective thermal conductivity, and examine the transient operational characteristics and performance limitations. These studies included a combined steady-state analytical and experimental investigation of a heat pipe approximately 1 mm$^2$ in cross-sectional area,[1] a transient numerical investigation of a similar device,[2] and an evaluation of individual micro heat pipes etched or cut into silicon wafers.[3]

In one of the first analytical investigations of these devices, Peterson[4,5] developed a steady-state model for trapezoidal micro heat pipes to predict the maximum heat transport capacity using the conventional steady-state modeling techniques outlined by Chi.[6] Somewhat later, a transient three-dimensional numerical model was developed by Peterson and Mallik[7] to determine the potential advantages of constructing an array of very small heat pipes as an integral part of semiconductor chips. Because of the high effective thermal conductivity, this array of heat pipes functions as a highly efficient heat spreader. Modeling results indicated that significant reductions in the maximum chip temperature, thermal gradients, and localized heat fluxes could be attained through the incorporation of this array of micro heat pipes. Concurrently, Khrustalev and Fagri[8] developed a one-dimensional model describing the fluid flow and heat and mass transfer in a microscale heat pipe with rectangular grooves to predict the capillary limitation and the point at which bubble incipience occurs. This model demonstrated reasonably good agreement with the limited experimental data of Plesch et al.[9]

Longtin et al.[10] investigated micro heat pipes with triangular grooves, using the one-dimensional model to predict the limitation of the heat pipe. This model, however, was limited to a determination of the flow conditions in the evaporator and adiabatic sections and neglected the effect and impact of the condenser section. Although this model may be applicable for situations with relatively short condenser sections, it is clearly not valid for the applications with very long condenser sections, similar to those of interest here. In addition, determination of the initial radius of the liquid meniscus in the evaporator was not clear in this model, and the physical meaning of the method by which the maximum heat transport capacity was determined was not clear.

Peterson and Ma[11] studied the maximum heat transport capacity and liquid pressure drop in triangular grooves based on the capillary limit. The uniform heat flux assumption in the evaporator employed in this model, although simplifying the problem, resulted in small errors that were compounded by the assumption of a constant radius of the curvature in the evaporator section.

Although a number of theoretical investigations have been conducted to predict the limitation of the micro heat pipes and operating characteristics, there is no general method that can be used for micro heat pipes with large variations in the size of the evaporator and condenser sections. The objective of this investigation is threefold: first, to develop an analytical model that can be used to predict the capillary limitation of the wire-bonded micro heat pipe; second, to determine the optimum operating characteristics and design parameters; and third, to determine the effect of variations in the geometric parameters on the maximum heat transport capacity.

## Theoretical Analysis

Figure 1 illustrates the overall size and geometric configuration of the wire-bonded micro heat pipe array presented here. The sharp corner regions formed between the wires and the sheets as illustrated in Fig. 1b are used as liquid arteries to pump the working fluid from the condenser section to the evaporator section. The vapor flows through the axial channels formed between the individual wires. To examine the effects of geometric parameters on the heat transfer performance, six micro heat pipes with different wire diameters and wire spacings were investigated in the current study. The physical specifications are listed in Table 1. In all six configurations, acetone was used as the working fluid.

Although micro heat pipes are very efficient heat transfer devices, they are subject to a number of heat transfer limitations. These limitations determine the maximum heat transport capacity that a particular heat pipe can achieve under certain operating conditions. The type of limitation that restricts the operation of a heat pipe is determined by which limitation has the lowest value at a specific heat pipe working temperature. Among the possible limitations on maximum axial heat transfer rates are the continuum flow limit, the frozen startup limit, the viscous limit, the sonic limit, the entrainment limit, the capillary limit, the condenser limit, and the boiling limit. Limitations to heat transport primarily arise from the inability

**Table 1 Configurations for the studied flat wire-bonded micro heat pipes**

| Prototype | Case 1 | Case 2 | Case 3[a] | Case 4[a] | Case 5[a] | Case 6 |
|---|---|---|---|---|---|---|
| Material | Aluminum | Aluminum | Aluminum | Aluminum | Aluminum | Aluminum |
| Working fluid | Acetone | Acetone | Acetone | Acetone | Acetone | Acetone |
| Total dimension, mm | 152.4 × 152.4 | 152.4 × 152.4 | 152.4 × 152.4 | 152.4 × 152.4 | 152.4 × 152.4 | 152.4 × 152.4 |
| Thickness of sheet, mm | 0.406 | 0.406 | 0.406 | 0.406 | 0.406 | 0.406 |
| Diameter of wire, mm | 0.330 | 0.406 | 0.635 | 0.813 | 1.016 | 1.270 |
| Number of wires | 108 | 96 | 77 | 84 | 73 | 59 |
| $w$, mm | 1.40 | 1.6 | 2.0 | 1.8 | 2.1 | 2.60 |
| Evaporator size, mm | 25.4 | 25.4 | 25.4 | 25.4 | 25.4 | 25.4 |
| Adiabatic section, mm | 93.0 | 93.0 | 93.0 | 93.0 | 93.0 | 93.0 |
| Condenser size, mm | 34.0 | 34.0 | 34.0 | 34.0 | 34.0 | 34.0 |
| Charging volume, ml | N/A | N/A | 1.8 | 2.9 | 4.3 | N/A |
| Thermocouples | N/A | N/A | 18 | 18 | 18 | N/A |

[a]Micro heat pipe arrays fabricated and tested.

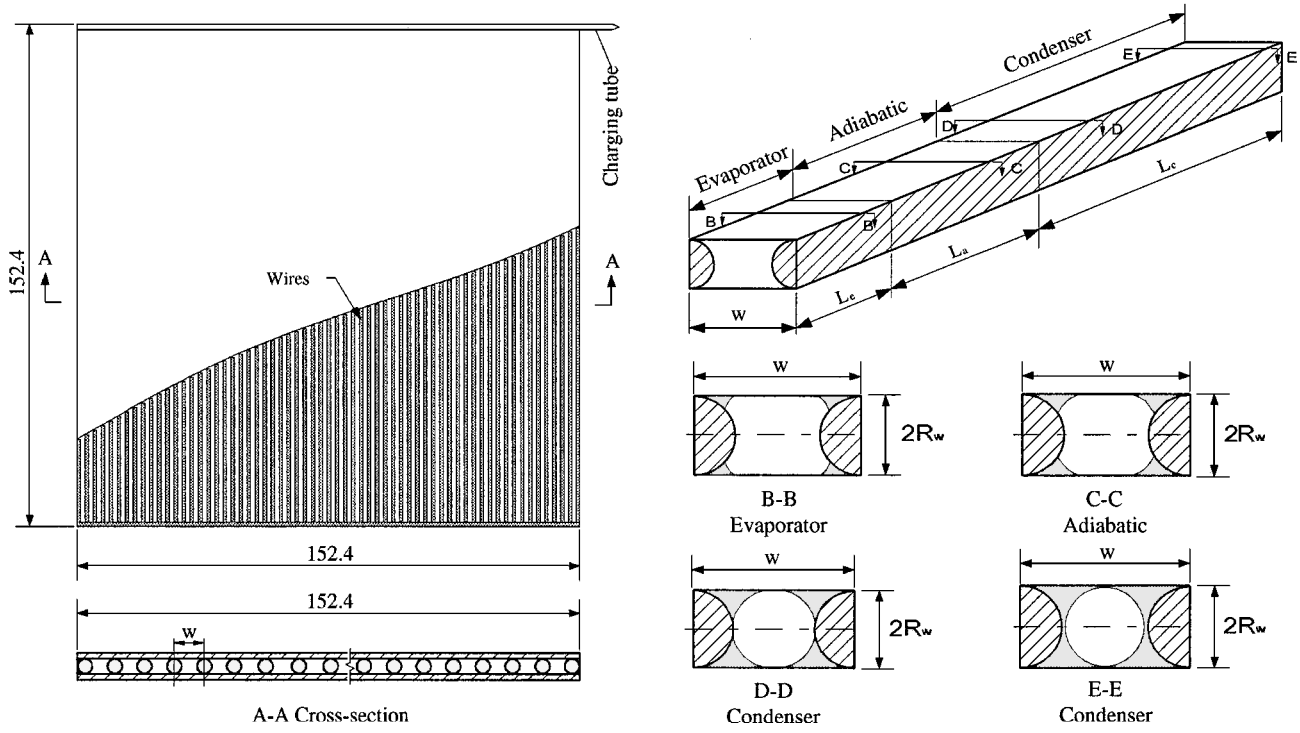


**a) Micro heat pipe array** **b) Micro channel in the array**

**Fig. 1 Flat wire-bonded micro heat pipe.**

of the wick to return the condensate to the evaporator and from the thermodynamic barriers encountered in the flow of the vapor. Among these limitations, the capillary limitation is dominant in low to moderate temperature heat pipes similar to those of interest in the present study.[4,5,12] As a result, the following analytical model focuses on the capillary limitation.

### Fluid Flow in Microchannel

The cross section of the micro heat pipe formed by two thin sheets and two parallel wires is shown in detail in Fig. 1b. During steady-state operation, evaporation in the evaporator and condensation in the condenser cause the working fluid to recede into the corners of the evaporator and flood the condenser section. The combination of these two phenomena generates the necessary capillary pressure to pump the working fluid from the condenser to the evaporator. Hence, the interfacial radius of curvature, which is directly related to the pressure difference between the liquid and vapor phase by the Laplace–Young equation

$$P_v(x) - P_l(x) = \sigma / r_m(x) \tag{1}$$

is of critical importance. This relationship can be expressed in differential form with respect to the axial position $x$ as

$$\frac{\mathrm{d}P_v}{\mathrm{d}x} - \frac{\mathrm{d}P_l}{\mathrm{d}x} = -\frac{\sigma}{r_m^2}\frac{\mathrm{d}r_m}{\mathrm{d}x} \tag{2}$$

Because of the viscous friction of the vapor flow, the vapor pressure will vary from the evaporator to the condenser and will result in a temperature variation due to the saturated vapor flow. Based on the Clausius–Clapeyron equation, this vapor temperature variation can be expressed as

$$T_v = \frac{T_{v,0}}{1 - (R_g T_{v,0}/h_{fg})\ln(P_v/P_{v,0})} \tag{3}$$

### Mass Conservation

The two-phase flow and heat transfer occurring in the microchannels are governed by mass, momentum, and energy conservation. During steady-state operation, the time rate of change of mass in both the liquid and vapor control volume is zero. The mass conservation equation for the liquid and vapor can be expressed as

$$\frac{\mathrm{d}\dot{m}_l}{\mathrm{d}x} - \rho_l v_{i,l} p_{i,l} = 0 \tag{4}$$

$$\frac{\mathrm{d}\dot{m}_v}{\mathrm{d}x} - \rho_v v_{i,v} p_{i,v} = 0 \tag{5}$$

The interfacial perimeters depend on the geometry of the wick structure, and the interfacial velocities can be obtained from the energy conservation equations.

### Momentum Conservation

Conservation of linear momentum in the liquid control volume consists of several parts, including the difference between the inflow and outflow momentum in the control volume, the body force term, that is, gravity, and surface forces (normal and tangential components). When these terms are combined, the momentum equation for the liquid yields

$$-\left[\dot{m}_l\frac{\mathrm{d}u_l}{\mathrm{d}x} + u_l\frac{\mathrm{d}\dot{m}_l}{\mathrm{d}x}\right] - A_{c,l}\frac{\mathrm{d}P_l}{\mathrm{d}x} + p_{i,l}\tau_{i,l} + p_{w,l}\tau_{w,l} - g\rho_l A_{c,l}\sin\theta = 0 \tag{6}$$

where $\dot{m}_l = \rho_l u_l A_{c,l}$.

Similarly, the momentum conservation equation for vapor phase yields

$$\dot{m}_v\frac{\mathrm{d}u_v}{\mathrm{d}x} + u_v\frac{\mathrm{d}\dot{m}_v}{\mathrm{d}x} + A_{c,v}\frac{\mathrm{d}P_v}{\mathrm{d}x} + p_{i,v}\tau_{i,v} + p_{w,v}\tau_{w,v} + g\rho_v A_{c,v}\sin\theta = 0 \tag{7}$$

where $\dot{m}_v = \rho_v u_v A_{c,v}$.

To compute the shear stresses, both the liquid and vapor flows are assumed to be fully developed duct flow, which is justified because of the small convective terms and the small changes in the liquid and vapor cross-sectional areas with respect to $x$.

**Energy Conservation**

Heat is transported through phase change in the heat pipe, and the thermal resistance of the phase change is very small when compared with the conduction resistance of the liquid phase and metal case material along the length of the heat pipe. Because the liquid film is so thin, and the Reynolds numbers are so low, convection and viscous dissipation in the liquid may be neglected. Basically, any energy input into the control volume manifests itself through either vaporization or condensation at the interface. As a result, conservation of energy for the liquid can be expressed as

$$v_{i,l} = \frac{2q''w}{\rho_l p_{i,l} h_{fg}} \tag{8}$$

where $q''$ is the heat flux added in the evaporator region or removed in the condenser region.

When the heat addition and removal are assumed to occur uniformly from the evaporator and condenser sections, respectively, and it is assumed that there is no heat loss in the adiabatic section, the interfacial velocity can be shown to be

$$v_{i,l} = \begin{cases} \dfrac{2q_e''w}{\rho_l p_{i,l} h_{fg}} & \text{evaporator section} \\ 0 & \text{adiabatic section} \\ \dfrac{2q_c''w}{\rho_l p_{i,l} h_{fg}} & \text{condenser section} \end{cases} \tag{9}$$

Similarly, the energy conversation equation for the vapor phase is given as follows:

$$v_{i,v} = \begin{cases} \dfrac{2q_e''w}{\rho_v p_{i,v} h_{fg}} & \text{evaporator section} \\ 0 & \text{adiabatic section} \\ \dfrac{2q_c''w}{\rho_v p_{i,v} h_{fg}} & \text{condenser section} \end{cases} \tag{10}$$

To solve Eqs. (2) and (4–7) with the appropriate boundary conditions, the cross-sectional areas of the liquid and vapor phases and the solid–liquid and liquid–vapor interfacial perimeters must all be known.

Based on the geometry of the cross section of the micro heat pipe as shown in Fig. 2, the liquid distribution profile in the microchannel formed between the two wires and the sheets depends on the diameter of the wire and the properties of the working fluid. For capillary flow at very low Reynolds numbers, the free surface will have a nearly constant radius of curvature, dependent primarily on the geometric shape of the liquid flow passage. Therefore, the liquid–vapor interface profile can be assumed to be a section of the round circle. The relationship of the wire diameter, meniscus radius, and contact angle can be determined from the geometry of the flow passage as

$$\beta_1 + \beta_2 + \alpha = \pi/2 \tag{11}$$

$$R_w \sin^2 \beta_1 = r_m \cos\beta_1 \sin\beta_2 \tag{12}$$

where $\beta_1$ the half-angle of the wire wall liquid and $\beta_2$ the half-angle of the meniscus curvature. The solutions of Eqs. (11) and (12) were determined as

$$\beta_1 = a\tan\left((1/2R_w)\left\{-r_m \sin\alpha + \left[(r_m \sin a)^2 + 4R_w r_m \cos\alpha\right]^{\frac{1}{2}}\right\}\right) \tag{13}$$

$$\beta_2 = \pi/2 - \alpha - a\tan\left((1/2R_w)\left\{-r_m \sin\alpha + \left[(r_m \sin a)^2 + 4R_w r_m \cos\alpha\right]^{\frac{1}{2}}\right\}\right) \tag{14}$$

The perimeter of the liquid–vapor interface, the liquid–solid contact line, and the liquid cross-sectional area can be expressed as

$$p_l = 2R_w(\beta_1 + \tan\beta_1) \tag{15}$$

$$p_v = 2(w + \pi R_w) + 8(r_m\beta_2 - R_w \tan\beta_1 - R_w\beta_1) \tag{16}$$

$$p_{i,l} = p_{i,v} = 8r_m\beta_2 \tag{17}$$

The liquid flow cross-sectional area and vapor flow cross-sectional area can be expressed as

$$A_{c,l} = 2R_w r_m \sin\beta_1 \sin\beta_2 - R_w^2(\beta_1 - \sin\beta_1\cos\beta_2) - r_m^2(\beta_2 - \sin\beta_2\cos\beta_2) \tag{18}$$

$$A_{c,v} = R_w(2w - \pi R_w) - 4A_{c,l} \tag{19}$$

The hydraulic diameter of the liquid and vapor flow areas can then be found to be

$$D_{h,v} = 4A_{c,v}/p_v \tag{20}$$

$$D_{h,l} = 4A_{c,l}/p_l \tag{21}$$

**Liquid and Vapor Friction Factors**

To solve the momentum equation, the liquid and vapor friction factors must be determined. The interfacial stresses in Eqs. (6) and (7) can be expressed by either the vapor or liquid friction factor as

$$\tau_{v,i} = f_{vi}\tfrac{1}{2}\rho_v u_v^2 \tag{22}$$

$$\tau_{l,i} = f_{li}\tfrac{1}{2}\rho_l u_l^2 \tag{23}$$

When it is assumed that there is no slip at the interface,

$$\tau_{v,i} = \tau_{l,i} \tag{24}$$

Because of the existence of counterflow, the interaction between the liquid and vapor flow grows nonlinearly with increases in velocity. This effect is especially large in open longitudinal grooved capillary structures and can lead to difficulty in starting up the heat pipe for heat removal in the evaporation zone without thermal isolation of the remaining parts of the heat pipe.[13] The interfacial stress coefficient for various groove shapes depends on the properties of the working fluid, the velocity difference of the liquid and vapor, and the geometric shape of the wick structure. Ma et al.[14] investigated the liquid–vapor interface interaction in triangular grooves. A dimensionless vapor–liquid interface flow number was introduced to characterize the effect of the vapor flow on the liquid flow. However, it is very difficult to determine the average surface velocity of the liquid, and, thus, this value is not normally utilized directly, except for special cases.

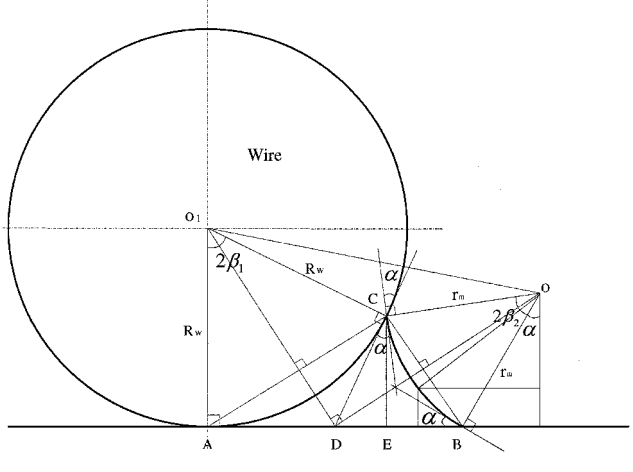


**Fig. 2 Geometry of the liquid meniscus in the microchannel.**

However, employing the experimental results and combining the shape factor, the liquid friction factor for any triangular groove can be approximated as

$$f_l Re_{h,l} = (f_l Re_{h,l})_0\left(1 + 0.0002 Re_{h,v}\left(\tfrac{1}{2} + \xi\right)\right) \tag{25}$$

where $Re_{h,v}$ is the Reynolds number of the vapor phase and $(f_l Re_{h,l})_0$ is the friction factor of the liquid phase when there is no vapor flow effect. From the data provided by Shah and Bhatti,[15] a general correlation can be obtained and expressed as

$$(f_l Re_{h,l})_0 = 12.0(1 + 0.5162\xi - 0.8018\xi^2 + 0.4177\xi^3) \tag{26}$$

where the shape factor is defined as

$$\xi = W/2H \tag{27}$$

$W$ and $H$ are the width and height of the triangle, respectively.

The sharp corner formed between the thin metal sheets and the wires is an irregular triangle, and the friction factor can be estimated using a technique proposed by Bejan[16]:

$$(f_l Re_{h,l})_{\text{wire}} = \psi (f_l Re_{h,l}) \tag{28}$$

where $\psi$ is a shape factor for this irregular figure, defined as

$$\psi = \frac{8[1 + \sin(\beta_1/2)]^2}{\sin\beta_1}\frac{A_{c,l}}{p_l^2} \tag{29}$$

This shape factor is used to correct the liquid friction factor in this case.

Because of the evaporation occurring in the evaporator and the condenser regions, the shape of the cross section varies all along the longitudinal axis of the heat pipe, as does the vapor velocity. For this reason, the vapor friction factor is difficult to express explicitly. At the end of the condenser, the cross section is almost a circle, and in the middle region of the heat pipe it can be more closely approximated by a rectangle. For both regions, the friction factor can be approximated using the approach developed by Bejan.[16]

### Boundary Conditions

Equations (2) and (5–8) constitute a set of five first-order, nonlinear, coupled ordinary differential equations in five unknowns: $r_m$, $u_v$, $u_l$, $P_v$, and $P_l$. Boundary conditions are needed at only one point for the solution to proceed; thus, the set of equations represents an initial value problem. The solution begins from the end of the condenser and proceeds to the evaporator section. The initial conditions for the adiabatic section equations are taken from the solution of the condenser at the condenser–adiabatic interface. The adiabatic and evaporator interface transition is handled in a similar manner.

The boundary conditions used at the end of condenser, $x = L_t$, are

$$u_l = u_v = 0 \tag{30}$$

$$r_m = r_{m,\max} \tag{31}$$

$$P_v = P_{\text{sat}}(T_v) \tag{32}$$

$$P_l = P_v - \sigma/r_{m,\max} \tag{33}$$

Here, $P_v$ is taken to be the saturation pressure of the vapor at $T_v$. The maximum meniscus radius occurs at the end of the condenser farthest from the evaporator. When the film condensate meets at the midpoint of the wire, the meniscus reaches a maximum value that can be expressed as

$$r_{m,\max} = R_w/(\cos\alpha - \sin\alpha) \tag{34}$$

It is clear that the maximum meniscus radius depends primarily on the diameter of the wire and increases proportionally with increasing wire diameter, as shown in Fig. 3a. The contact angle of the liquid on the case wall also has a significant effect. As shown in Fig. 3b, the maximum meniscus radius increases with increasing contact angle. When the contact angle is less than 20 deg, the influence is very small, but as the contact angle increases, the velocity increases to a point where, when the contact angle reaches a value greater than 35 deg, the maximum meniscus increases sharply.

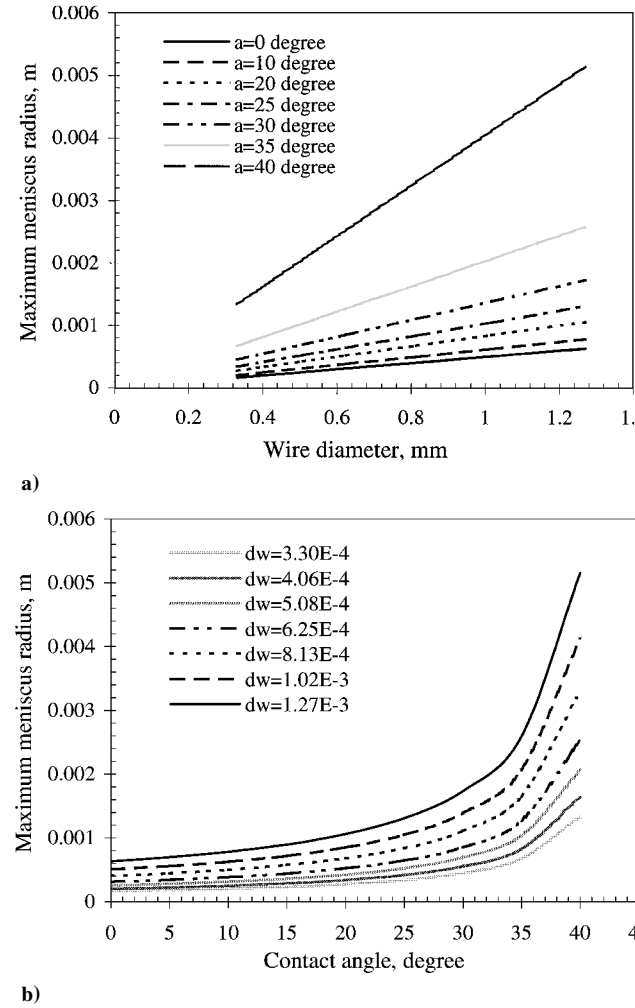


**Fig. 3 Effect of a) the wire diameter and b) the contact angle on the maximum meniscus radius.**

To find the maximum heat transport capacity, the minimum meniscus radius must be determined. Because the exact evaporation process of the liquid in the microchannel at the maximum heat flux is not clear, it is difficult to determine precisely the minimum meniscus radius in the evaporator. Several authors[1,17,18] have estimated the minimum meniscus radius in a particular micro heat pipe based on different approaches; however, no general method for computing this value has been developed. Here, it is assumed that, when the heat input in the evaporator section is larger than the maximum capillary heat transport capacity, dry out will occur in the evaporator section of the micro heat pipe.

When it is assumed that the maximum heat power added to the evaporator section is $Q_{\max}$, at any point where the heat pipe is operating properly, and right up to the point just before dry out, the amount of liquid vaporized will be equal to the amount of liquid pumped into the control volume. The amount of working fluid flowing into the control volume can be shown to be

$$4V_c\rho_l h_{fg} = (Q_{\max}/2wL_e)2w\,\mathrm{d}z \tag{35}$$

where $V_c$ is the volume of one corner, which, from the geometry shown in Fig. 2, can be expressed as

$$V_c = \left\{2R_w r_m \sin\beta_1 \sin\beta_2 - R_w^2(\beta_1 - \sin\beta_1\cos\beta_1) - r_m^2(\beta_2 - \sin\beta_2\cos\beta_2)\right\}\mathrm{d}z \tag{36}$$

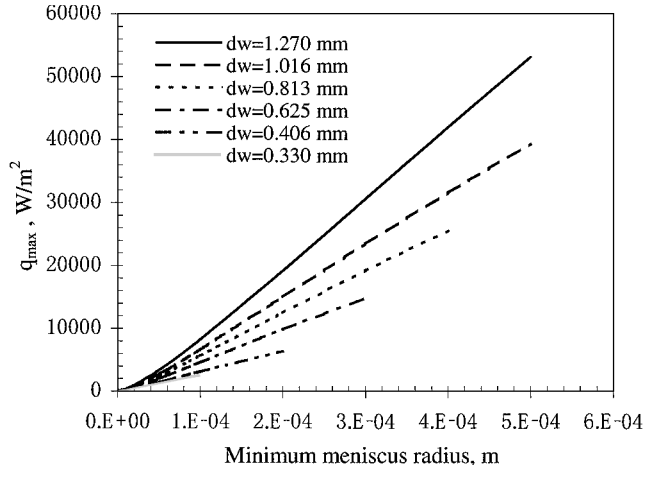


a)

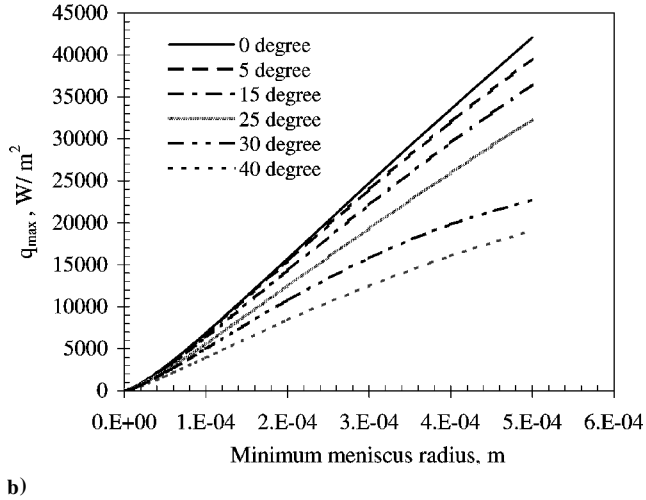


b)

**Fig. 4 Effect of a) the wire diameter and b) the contact angle on the minimum meniscus radius.**

When Eq. (36) is substituted into Eq. (35), and then rearranged, the minimum meniscus radius can be expressed as

$$2R_w r_m \sin\beta_1 \sin\beta_2 - R_w^2(\beta_1 - \sin\beta_1 \cos\beta_1) - r_m^2(\beta_2 - \sin\beta_2 \cos\beta_2) = Q_{\max}/4L_e\rho_l h_{fg} \quad (37)$$

The minimum radius of the meniscus can be obtained from the energy balance, Eq. (37). It can be shown that the minimum radius of curvature depends on the heat flux, the geometric shape of the grooves, and the properties of working fluid. The effect of contact angle, wire diameter, and heat flux on the minimum meniscus radius of the curvatures is illustrated in Figs. 4a and 4b. When the contact angle increases, the maximum heat flux (maximum heat transport capacity) decreases. Note that Eq. (37) is used only to determine the minimum radius of curvature that corresponds to the maximum heat transport for a special micro heat pipe with given conditions.

### Numerical Treatment

The five first-order differential equations (2) and (4–7) and the associated boundary conditions described by Eqs. (30–33) can be solved numerically for the five unknowns, $r_m$, $u_v$, $u_l$, $P_v$, and $P_l$, using a fourth-order Runge–Kutta method. In the case of a condenser exposed to a radiation environment, neither the heat flux nor the temperature is constant. The heat flux depends on the outside surface temperature of the heat pipe. It is impossible to know the initial temperature or pressure at the end of the condenser. Therefore, an initial temperature must be assumed and then the corresponding pressure, velocity, liquid profile, and heat transfer coefficient calculated. The total radiation power must then be compared to the power input in the evaporator section and the process iterated.

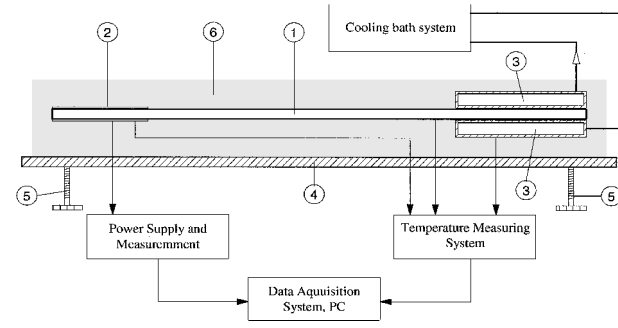


**Fig. 5 Experimental facility: 1, micro heat pipe; 2, electric film heaters; 3, cooling plates; 4, Lexan support plate; 5, adjustable feet; and 6, insulation.**

## Experimental Investigation

To verify the wire-bonded micro-heat-pipe concept and validate the proposed numerical model, several aluminum–acetone wire-bonded micro heat pipe arrays were fabricated and evaluated experimentally. The physical configuration and the charging quantity for each of the micro heat pipe arrays tested are presented in Table 1, and the experimental system is shown in Fig. 5. The system was composed of the micro heat pipe array, two electrical resistance film heaters, two cooling plates, an adjustable Lexan® plate, a power supply and measurement unit, a cooling bath, and a temperature measuring and data acquisition system. The operating temperature was controlled in a range of 20–80°C to within an uncertainty of ±0.71°C. The micro heat pipe array was divided into three distinct regions, the evaporator section, the adiabatic section, and the condenser section. Heat was added uniformly to the evaporator section and removed from the condenser section by cold plates. A cooling fluid was passed through the cold plates, and the heat was removed by forced convection. The power input and the temperature distributions on the outer surface of the micro heat pipe were measured to find the maximum heat transport capacity and effective thermal conductivity. To identify the effect of the geometry of the grooves on the maximum capillary transport capacity, several heat-pipe arrays with different wire diameters and channel widths were fabricated and tested.

Two electric film heaters were attached to the two sides of the evaporator. The length of the heaters was 152.4 mm, and the width was 25.4 mm. Power generated by the heaters was controlled by an autotransformer and measured by a power measuring system. The two cold plates that were constructed from aluminum 2024 (240 mm long and 34.0 mm wide) were attached to the outside surfaces of the condenser section of the micro-heat-pipe array. Cooling fluid flowed through the cold plates and removed the heat by forced convection. To enhance the thermal contact, a thin layer of silicone heat sink compound (Dow Corning 340) was placed between the cold plate and the micro heat pipe array. The cooling bath was set to the required temperature and held at a constant temperature throughout the tests. The temperature variation of the cooling fluid was held to within ±1°C. The micro heat pipe arrays were placed on a Lexan plate that could be adjusted to keep the array in a horizontal position or at the required angle. In the horizontal position, the effect of the force of gravity could be eliminated.

To monitor the temperature variation along the heat-pipe array, 24 thermocouples were attached to the surface of the micro heat pipe array and directly connected to an Hewlett–Packard Co. HP3497A data acquisition system controlled by a personal computer. In addition, two thermocouples were placed on the outer surface of the cold plate to monitor the cooling fluid temperature and ensure a constant condenser temperature.

Before each test, the system was allowed to equilibrate for approximately 1 h. The power supply was then turned on and the power incremented. At this point in the tests, it took approximately 20–30 min to reach steady state. The temperature distribution along the heat pipe was recorded when the measured temperatures did not vary by more than ±0.5°C in a 10-min period. The power input was then incrementally increased until dryout occurred. When dryout

was ultimately reached, as determined by the rapid increase in the temperatures at the end of the evaporator, the temperature difference between the evaporator and condenser increased quickly. The power input at this point was assumed to be the maximum heat transport capacity of the heat pipe at this operating temperature. When the cooling temperature was changed and the same procedures described followed, the maximum heat transport capacity at various operating temperatures was obtained.

For all of the tests, the measured heat loss was less than 9.6% of the power input to the evaporator by the heater. The uncertainty of the measured power input was approximately 0.58 W.

## Results and Discussion

Six different micro heat pipes with different wire diameters and wire separation distances were evaluated experimentally to determine the effects of these parameters on performance. During the tests and analysis, the micro heat pipe arrays were separated into three clearly distinct regions. Heat was added uniformly to the evaporator section by a thin-film heater over a length of 25.4 mm and removed from the condenser by cold plates attached to the outer surface over a length of 34.0 mm. The adiabatic section was assumed to be perfectly insulated (i.e., no heat loss in this section), and the total length was 152.4 mm. The physical configurations of the micro heat pipes investigated are listed in Table 1. To compare the theoretical predictions with the experimental results, the analytical model was modified slightly to conform more accurately to the experimental situation. Because the amount of working fluid strongly affects the maximum heat transport capacity and, as shown later, the distribution of the working fluid varies with the operating conditions, the predicted maximum heat transport capacity is based on an optimum fluid charge, and the physical properties of the working fluid, acetone, were determined as a function of the operating temperature.

### Pressure Distributions

In the operation of these devices, vapor flows from the evaporator to the condenser as a result of the temperature gradient and resulting pressure difference. As the vapor moves in the axial direction, the pressure decreases due to the viscous friction. The liquid returns from the condenser section to the evaporator section due to the capillary pressure, but also experiences a decrease as it moves in the axial direction, due to the frictional force. These trends are clearly illustrated in Fig. 6, which presents the axial pressure distribution for a micro heat pipe array with a wire diameter of 1.016 mm. As shown, the liquid pressure decreases very rapidly as the input heat flux increases due to the velocity increase and liquid cross-sectional area decrease. The vapor pressure, although experiencing some axial decrease, demonstrates much less variation in total pressure drop as the evaporator heat flux is varied.

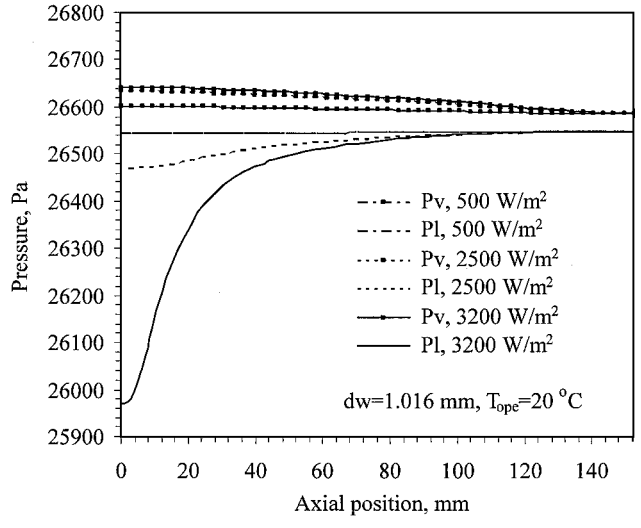


**Fig. 6 Pressure distributions in the micro heat pipe with $d_w$ = 1.016 mm.**

As discussed earlier, the difference in the curvature of the liquid meniscus between the evaporator and condenser provides the driving force behind the liquid transport. As shown in Fig. 7, the meniscus radius varies, both as a function of the axial position and also as a function of the evaporator heat flux. This variation in the curvature of the liquid meniscus decreases continuously from the condenser to the evaporator due to the capillary pressure required to overcome the pressure drop caused by friction. With increases in the evaporator heat flux, the meniscus radius at the end of the evaporator decreases continuously and finally reaches a minimum value when the heat transport reaches a maximum.

### Mass Distributions

Unlike large-scale heat pipes, micro heat pipes typically do not have a wick structure but rather use the sharp corners or grooves as liquid arteries. Therefore, it is difficult to estimate the precise quantity of the working fluid required for proper operation. The charge volume of the micro heat pipe depends on the mass distribution of the liquid in the microchannels, and the associated liquid mass distribution depends on the geometry of the channel, the heat transport, and the properties of the working fluid. The liquid meniscus radius changes continuously from the evaporator to the condenser, and the cross-sectional area of the liquid strongly depends on the liquid meniscus radius and the evaporator heat flux, as shown in Fig. 7. The cross-sectional area of the liquid phase decreases from the condenser to the evaporator, and the liquid distribution in the channel decreases with increasing power input, as illustrated in Fig. 8. This

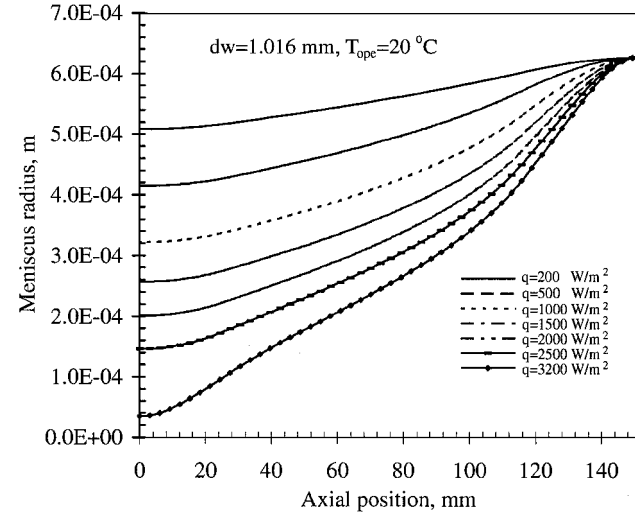


**Fig. 7 Variation of the liquid meniscus in the microchannel of the micro heat pipe with $d_w$ = 1.016 mm.**

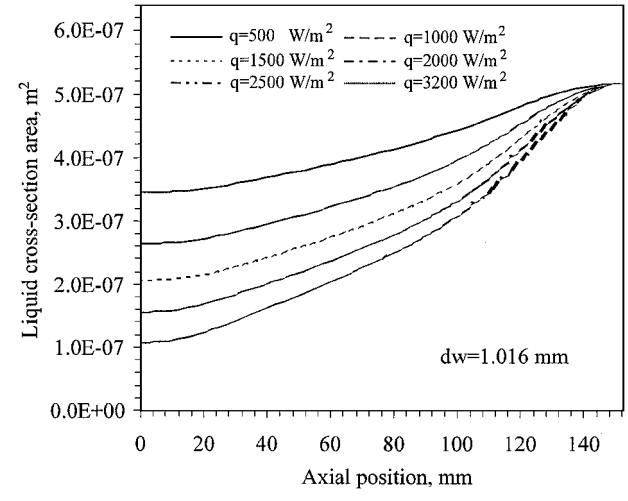


**Fig. 8 Liquid distribution in the micro heat pipe with variations in the heat flux.**

implies that the amount of working fluid required for proper operation of the micro heat pipe array varies. The ideal operating state of a heat pipe is to have no extra working fluid in the condenser section to block the effective condenser length. The optimum charging quantity can be determined by integrating the mass distribution in the channel from the end of the evaporation to the end of the condenser.

The optimal charging volume obtained from the model is presented in Fig. 9 as a function of the heat flux. As shown, the optimum charge decreases with increasing heat flux, and, for micro heat pipes with a wire diameter of 1.016 and 0.813 mm, the optimum charge is between 18.6 and 36.0% and 17.0 and 31.9% of the total volume of the channel, respectively. This corresponds to the charging volume used in the experimental tests. Because it is difficult to charge the heat pipe with the exact optimum volume, these devices are typically slightly overcharged.

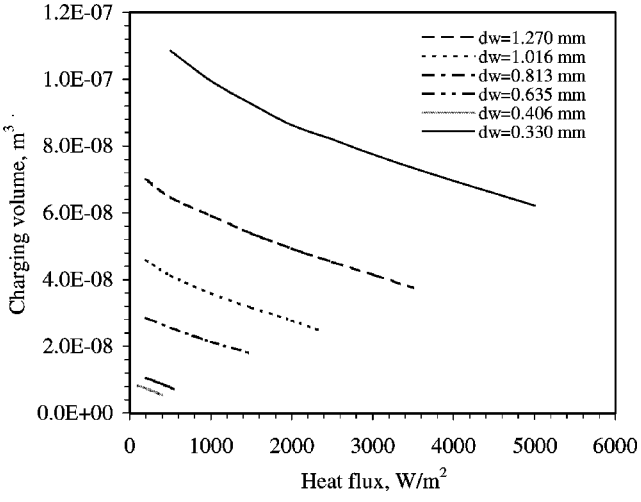


**Fig. 9 Optimum charging volume for the micro heat pipes.**

### Maximum Heat Transport Capacity

The maximum heat transport capacity of the micro heat pipe is reached when the capillary force created by the variation in the meniscus radii is equal to or less than the sum of the liquid and vapor frictional forces. In the experimental tests, this phenomenon was determined by recording the temperature variation on the surface of the micro heat pipe. As shown in Fig. 10, the temperatures at the end of the evaporator and the operating temperature (average adiabatic temperature) increased proportionally to the power input, and the operating temperatures rapidly approached the evaporator temperature. At the point where the temperature at the end of the evaporator increased sharply, dry out began, and the heat input at this point was assumed to be the maximum transport capacity corresponding to the operating temperature. The maximum heat transport capacity at various operating temperatures could be obtained by changing the cooling temperature in the condenser section.

The operating temperature, wire diameter, and the distance between the wires all have a significant effect on the maximum heat transport capacity. The effect of operating temperature on the micro heat pipes is presented in Fig. 11. As illustrated, the predicted maximum heat transport capacity increases with increases in operating

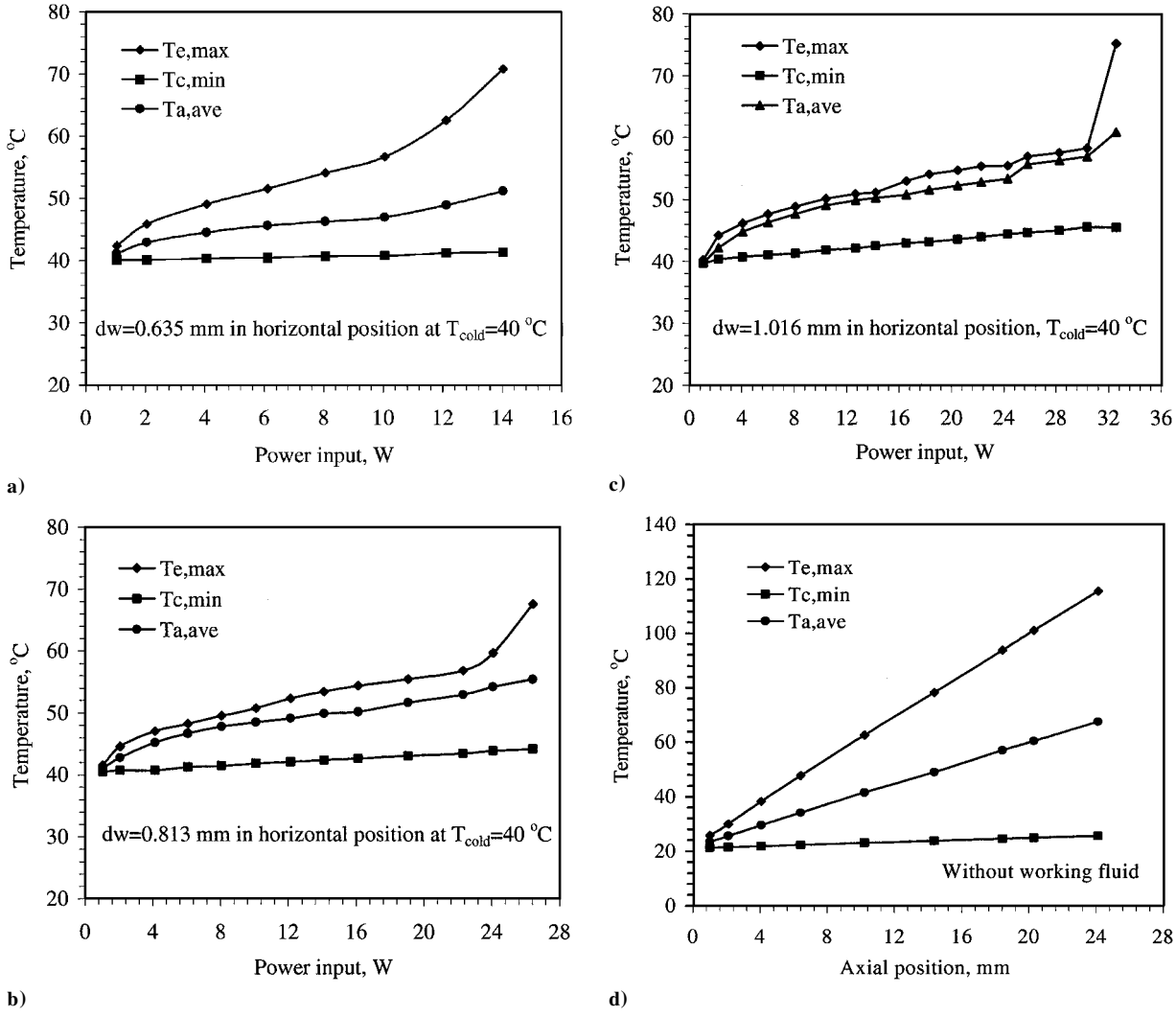


**Fig. 10 Temperature variations on the micro heat pipe with a) $d_w$ = 0.635 mm, b) $d_w$ = 0.813 mm, c) $d_w$ = 1.016 mm, and d) uncharged.**

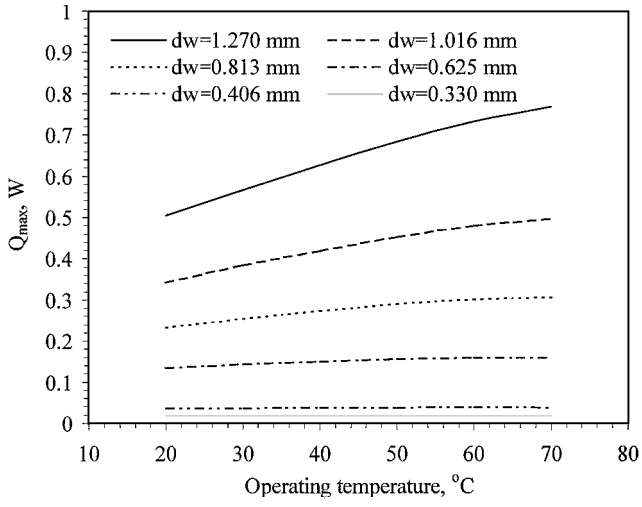


**Fig. 11 Predicted maximum heat transport capacities.**

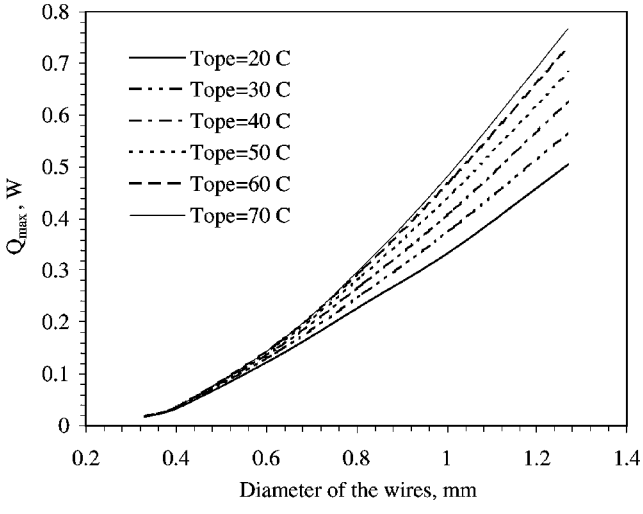


**Fig. 12 Variation of the maximum heat transport capacity with wire diameters.**

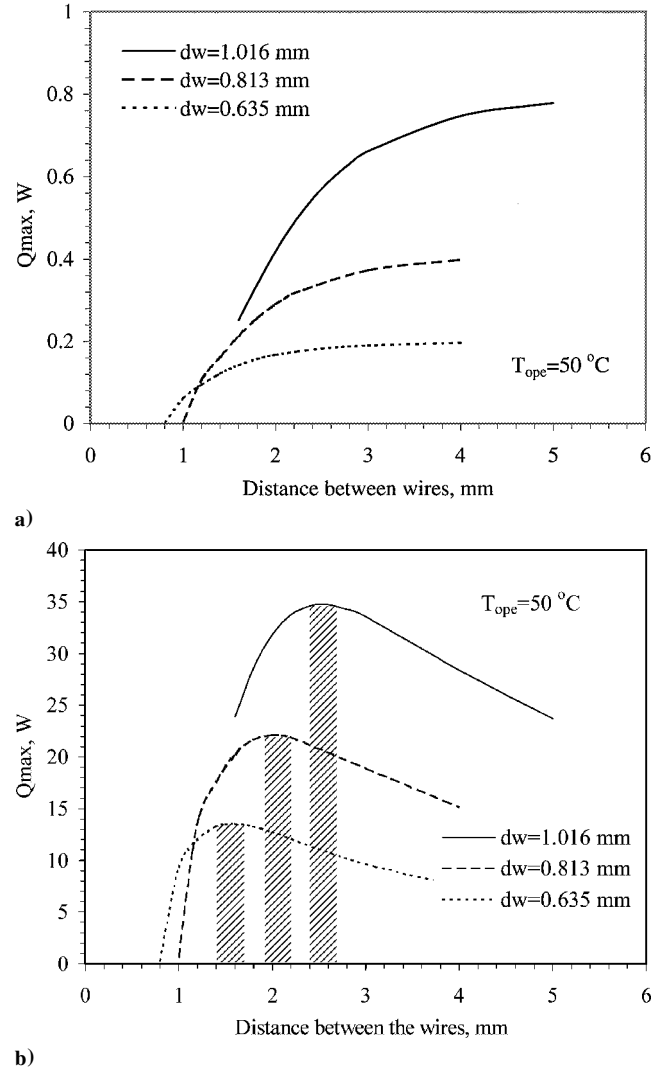


**Fig. 13 Effect of space distance on the maximum heat transport capacity of a) single micro heat pipes and b) micro heat pipe radiators.**

temperature. When the operating temperature increases to a predetermined value, the heat transport capacity reaches a maximum and then decreases slowly. This implies that there exists an optimum operating temperature at which point the heat transport will reach a maximum value. Furthermore, this optimum operating temperature increases with increases in wire diameter, that is, the optimum operating temperature is 50°C for $d_w = 0.33$ mm and about 70°C for $d_w = 0.635$ mm. This phenomenon is caused by the differing effects of temperature on the working fluid properties, most important on the viscosity and surface tension. At a lower average temperature, increases in temperature have a much greater effect on the viscosity than on the surface tension. However, at higher operating temperatures, the effect of temperature on the surface tension is more significant.

### Optimum Design Parameters

In addition to the operating temperature, both the wire diameter and the wire spacing can dramatically affect the maximum heat transport capacity. As shown in Fig. 12, the maximum heat transport capacity increases rapidly with increases in wire diameter. Analysis of the modeling results indicates that the maximum heat transport capacity is nearly proportional to the square of the wire diameter and has a value of only 0.0183 W for the micro heat pipe with a wire diameter of 0.33 mm. The estimated maximum heat transport capacity for this array is only 1.98 W. As observed in the preliminary experimental tests, this micro heat pipe array did not function properly for the range of test conditions evaluated here. Destructive evaluation of the array after testing indicated that the sharp corner regions, which normally serve as the liquid arteries, were filled with the brazing material during the fabrication process, limiting the capillary pumping capacity available and, as a result, decreasing the heat transport capacity.

The space between the two wires has a significant effect on the maximum heat transport capacity of micro heat pipes, because the cross-sectional area and the hydraulic diameter of the flow varies with the variation of the separation distance. As illustrated in Fig. 13a, the maximum heat transport capacity increases rapidly with increases in the width of the individual micro heat pipe, for example, the separation distance, due to the reduction in the viscous pressure drop. However, once the separation distance reaches a certain point, the rate of increase of the maximum heat transport capacity begins to decrease and levels off at a nearly constant value. Further increases in the separation distance only decrease the pressure drop of the vapor phase and do not have any additional affect on the pressure drop in the liquid phase.

For the flat-plate micro heat pipe arrays, the overall heat transport capacity depends on the combined maximum heat transport capacity of a series of individual heat pipes and, hence, on the total number of micro heat pipes. Increasing the distance between wires, although increasing the transport capacity of an individual heat pipe, may reduce the total transport capacity of the array due to a decrease in the number of the micro heat pipes in the array. This implies that there is an optimum distance at which point the maximum heat transport capacity of the array reaches maximum value. This

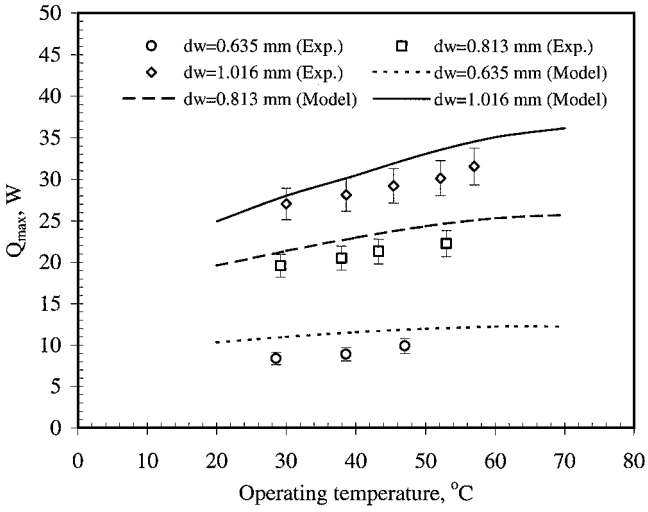


**Fig. 14 Comparison of the predicted and measured maximum heat transport capacity.**

relationship is illustrated in Fig. 13b, for micro heat pipe arrays with wire diameters of 1.016, 0.813, and 0.635 mm, where the optimum distance between the two wires is 2.5, 2.0, and 1.6 mm, respectively, or approximately 2.5 times the wire diameter.

#### Comparison of Measured and Predicted Performance

The predicted maximum heat transport capacities are compared with experimental results for the three micro heat pipes with wire diameters of 1.016, 0.813, and 0.635 mm. This comparison is shown in Fig. 14. As illustrated, the predicted values are slightly higher than the experimental values. The systematic overestimation may result from the partial filling of the sharp corners of the liquid arteries by the brazing material or the improper charging of the heat pipe array. The effect of the brazing material is more significant for micro heat pipes with smaller diameters. The maximum deviation is about 20.4% and occurs at the lowest operating temperature for the array with the smallest wire diameter. Overall, the analytical results are in very good agreement with the experimental results. The variation that does occur could be the result of a slight filling of the sharp corner regions of the grooves that occurred during the fabrication process, or due to variations in the charge volume from the optimal value.

## Conclusions

The heat transfer performance of wire-bonded aluminum–acetone micro heat pipe arrays has been investigated both analytically and experimentally. The mass distribution, the optimum charging quantity, the maximum heat transport capacity, and the effect of the wire diameter and the separation distance of the wires on the maximum heat transport capacity were evaluated. It was found that maximum heat transport capacity increases with increases in the wire diameter and is proportional to the square of the wire diameter. The maximum heat transport capacity also increases with increases in the operating temperature to a maximum value and then decreases within the operating temperature range of the working fluid. There exists an optimum operating temperature at which the maximum heat transport capacity reaches a maximum value. This optimum operating temperature increases with the increase in wire diameter.

Increasing the width of the micro heat pipe, for example, the separation distance, can increase the maximum heat transport capacity of single micro heat pipe. However, at some point, this improvement is overshadowed by the decrease in the number of heat pipes in the array, and the maximum heat transport capacity of the entire array becomes limited, implying that the maximum heat transport capacity of the flat micro heat pipe array depends not only on the maximum heat transport capacity of a single micro heat pipe, but also on the total number of the micro heat pipes in the array. In the current study, the optimum distance between two wires for micro heat pipes with wire diameters of 1.016, 0.813, and 0.635 mm were 2.5, 2.0, and 1.6 mm, respectively, or approximately 2.5 times the wire diameter. From the mass distribution of the liquid in the microchannel, the optimum charging volume was determined. This optimum charging volume decreased with increasing heat flux.

To validate the analytical model, the predicted results were compared with the experimental results. The relatively good agreement between the predicted and measured results validates the modeling and confirms that it can be used to accurately predict performance and optimize the design to achieve the maximum heat transport capacity for a given application.

## Acknowledgments

The authors would like to acknowledge the support of the National Science Foundation and the Office of Naval Research for the support of this work.

## References

[1] Babin, B. R., Peterson, G. P., and Wu, D., "Steady-State Modeling and Testing of a Micro Heat Pipe," *Journal of Heat Transfer*, Vol. 112, No. 3, 1990, pp. 595–601.

[2] Wu, D., and Peterson, G. P., "Investigation of Transient Characteristics of Micro Heat Pipes," *Journal of Thermophysics and Heat Transfer*, Vol. 2, No. 5, 1991, pp. 129–134.

[3] Peterson, G. P., Duncan, A. B., and Weichold, M. H., "Experimental Investigation of Micro Heat Pipe Fabricated in Silicon Wafers," *Journal of Heat Transfer*, Vol. 11, No. 3, 1993, pp. 751–756.

[4] Peterson, G. P., "Analytical and Experimental Investigation of Micro Heat Pipe," *Proceedings of the 7th International Heat Pipe Conference*, Luikov Heat and Mass Transfer Inst., Byelorussian Academy of Sciences, Minsk, USSR, May 1990, Paper A-10.

[5] Peterson, G. P., "An Introduction to Heat Pipes," *Proceedings of the 7th International Heat Pipe Conference*, Luikov Heat and Mass Transfer Inst., Byelorussian Academy of Sciences, Minsk, USSR, 1990, Paper A-4.

[6] Chi, S. W., *Heat Pipe Theory and Practice*, McGraw–Hill, New York, 1976, pp. 33–77.

[7] Peterson, G. P., and Mallik, A. K., "Transient Response Characteristics of Vapor Deposited Micro Heat Pipe Arrays," *Journal of Electronic Packing*, Vol. 117, No. 1, 1995, pp. 82–87.

[8] Khrustalev, D., and Fagri, A., "Thermal Analysis of Micro Heat Pipe," *Journal of Heat Transfer*, Vol. 116, No. 1, 1994, pp. 189–198.

[9] Plesch, D., Bier, W., Seidel, D., and Schubert, K., "Miniature Heat Pipes for Heat Removal from Microelectronic Circuits," *Proceedings of the ASME Annual Meeting*, American Society of Mechanical Engineers, Fairfield, NJ, 1991.

[10] Longtin, J. P., Badran, B., and Gerner, F. M., "A One-Dimensional Model of Micro Heat Pipe During Steady-State Operation," *Journal of Heat Transfer*, Vol. 116, No. 3, 1994, pp. 709–715.

[11] Peterson, G. P., and Ma, H. B., "The Theoretical Analysis of the Maximum Heat Transport in Triangular Grooves—A Study of Idealized Micro-Heat Pipes," *Journal of Heat Transfer*, Vol. 118, No. 3, 1996, pp. 731–739.

[12] Ma, H. B., and Peterson, G. P., "Experimental Investigation of Thermal Capillary Limit of a Novel Micro Heat Pipe Design," AIAA Paper 97-0979, Jan. 1997.

[13] Kemme, J. E., "Heat Pipe Capability Experiments," *Proceedings of the IEEE Thermionic Conversion Specialist Conference*, Inst. of Electrical and Electronics Engineers, Piscataway, NJ, 1966, pp. 159–168.

[14] Ma, H. B., Peterson, G. P., and Lu, X. J., "The Influence of Vapor–Liquid Interactions on the Liquid Pressure Drop in Triangular Microgrooves," *International Journal of Heat and Mass Transfer*, Vol. 37, No. 15, 1994, pp. 2211–2219.

[15] Shah, R. K., and Bhatti, M. S., "Laminar Convective Heat Transfer in Ducts," *Handbook of Single-Phase Convective Heat Transfer*, Wiley, New York, 1987, pp. 3.45–3.70.

[16] Bejan, A., *Convection Heat Transfer*, Wiley, New York, 1985, pp. 77–82.

[17] Cotter, T. P., "Principles and Prospects of Micro Heat Pipes," *Proceedings of the 5th International Heat Pipe Conference*, Tsukuba, Japan, 1984, pp. 328–335.

[18] Hopkins, R., Faghri, A., and Khrustalev, D., "Flat Miniature Heat Pipes with Micro Capillary Grooves," *Journal of Heat Transfer*, Vol. 121, No. 1, 1999, pp. 102–109.